537685

TDA Progress Report 42-102

August 15, 1990

N91-11975

Computer Simulations of Ions in Radio-Frequency Traps

A. Williams, J. D. Prestage, L. Maleki,
J. Djomehri, and E. Harabetian
Communications Systems Research Section

The motion of ions in a trapped-ion frequency standard affects the stability of the standard. In order to study the motion and structures of large ion clouds in a radio-frequency (rf) trap, a computer simulation of the system that incorporates the effect of thermal excitation of the ions has been developed. Results are presented from the simulation for cloud sizes up to 512 ions, emphasizing cloud structures in the low-temperature regime.

I. Introduction

The development of the trapped-ion frequency standard at the Jet Propulsion Laboratory (JPL) is motivated by the potential of this device to achieve stability exceeding one part in 10^{17}. The basis of the potential for this remarkable stability performance is the isolation of the trapped ions from perturbing influences that diminish stability over averaging intervals greater than several hundred seconds. In conventional frequency standards such as hydrogen masers, these effects include the interaction of the atoms with confining walls and phase-destructive collisions of atoms of the same species that are in different energy states.

The confinement of ions in rf traps (the type employed in the JPL trapped-ion standard) is accomplished by exposing the ions to an oscillating field, resulting in a force that acts to direct the ions toward the center of the trap and away from the trap electrodes. This electromagnetic containment is dynamic in nature, as will be detailed below. Therefore, since a large source of frequency offset is the second-order Doppler or relativistic time-dilation effect due to the motion of the ions, it is appropriate to study the dynamic effects in the rf trap system.

Ions, of course, do not lend themselves to easy visual observation, so the dynamics of trapped particles are often indirectly studied through the observation of the motion of micron-sized particles in a similar trap [1] or by computer simulations of the confining fields and Coulomb interactions experienced by ions in a trap. The introduction of computer simulations to the field of trapped-ion dynamics brings with it a new set of results, which are not from a laboratory experiment but from "computational" studies of a model. Naturally, if the model is an accurate representation of the real system at hand, a computer simulation using that model should duplicate behavior seen in experiments and that predicted by an accurate theory.

This article presents a study that uses computer simulation to examine the motion of ions confined in rf traps to determine possible influences on the frequency stability. While similar studies have been carried out for the case of

a few ions confined in rf traps, the present work includes results for clusters with as many as 512 ions. Thus, this study is a more realistic model for actual frequency standards, where the typical number of confined ions ranges from 10^3 to 10^6.

After a brief review of trapped-ion theory in Section II and a description of the simulation in Section III, the computational results are compared with theory in Section IV and with experiment in Section V. In Section VI, the JPL simulation is compared to the results from trapped-ion simulations carried out by other groups, and Section VII outlines the plans for using this simulation to further investigate trapped-ion dynamics.

II. Trapping Theory

The detailed theory of rf ion traps has been treated previously [2,3,4]. An outline of the theory is presented here to support the discussion of the computer model.

A Paul-type rf trap consists of three hyperbolic electrodes, as shown in Figs. 1(a) and (b).[1] Typically, these electrodes are arranged so that the radius of the trap cavity r_0 is $\sqrt{2}$ times the height of the cavity. An ac voltage with angular frequency Ω is applied in series with a dc voltage between the ring electrode and the two endcap electrodes.

Another type of trap, known as the Penning or dc trap, is described later in this article. Since a full development is not necessary in this discussion, the reader is referred to [2] and [3]. The Penning trap uses the same electrode configuration as the Paul trap, but the rf portion of the electric field is replaced by a static magnetic field in the z-direction. Hence, neither of the fields in this trap is time-varying.

Applying the Paul trap potentials produces a potential inside the trap of the form

$$\phi(r,z) = \frac{V_{DC} + V_{AC}\cos(\Omega t)}{2r_0^2}(r^2 - 2z^2) \qquad (1)$$

The electric field components are obtained by differentiating Eq. (1) as

$$\mathbf{E} = -\left(\frac{V_{DC}}{r_0^2} + \frac{V_{AC}\cos(\Omega t)}{r_0^2}\right)(\mathrm{r} - 2\mathrm{z}) \qquad (2)$$

[1] The linear rf trap described in [8] employs fields similar to the Paul trap, but consists of four cylindrical rods rather than the hyperbolic electrodes.

The trapping effect of this field configuration can be understood as follows. A node exists at the center of the trap ($r = z = 0$) where the electric field is zero; thus, there is no force on a charged particle located there. Depending on the sign of the rf term, at any given time the field is pointing toward the node in one direction and away from the node in the other. It can also be seen in Eq. (2) that the field magnitude increases with increasing distance from the node. This behavior of the field in the interior of the trap leads to a net force that, when averaged over one rf cycle, is directed toward the node [1]. This "ponderomotive" [5] force is what draws charged particles toward the node, trapping them inside the electrodes.

The equations of motion of a single ion subject to the force due to the electric field in Eq. (2) can be expressed using the two dimensionless constants

$$a = \frac{4eV_{DC}}{m\Omega^2 r_0^2} \qquad q = -\frac{2eV_{AC}}{m\Omega^2 r_0^2} \qquad (3)$$

to represent the trapping parameters, and a dimensionless time parameter

$$\tau = \frac{\Omega}{2}t \qquad (4)$$

In this formulation, the equations of motion become forms of the Mathieu differential equation

$$\frac{d^2r}{d\tau^2} = -(a - 2q\cos(2\tau))r \qquad (5)$$

for either radial dimension (x or y), and

$$\frac{d^2z}{d\tau^2} = 2(a - 2q\cos(2\tau))z \qquad (6)$$

for the axial dimension z. In the expressions for a and q, e and m denote the charge and mass of the contained particle, respectively.

The solutions of Eqs. (5) and (6) reveal that an ion influenced by the fields of a Paul trap undergoes a fast rf motion with the same frequency Ω as the driving ac potential, and a slow "secular" oscillation, which in the one-dimensional case carries it back and forth through the trap node.

When more than one ion of the same charge-to-mass ratio is present in the trap, each ion has its own equation of motion, consisting of a trapping term as above and a

Coulomb term containing the electrostatic interaction of all other ions. The motion in Cartesian coordinates x, y, and z of singly ionized atoms of mass m is described by the set of differential equations

$$\frac{d^2x_i}{d\tau^2} = -\big(a - 2q\cos(2\tau)\big)x_i - \frac{e^2}{\pi\epsilon_0 m\Omega^2}\sum_j \frac{(x_j - x_i)}{r_{ij}^3} \quad (7)$$

$$\frac{d^2y_i}{d\tau^2} = -\big(a - 2q\cos(2\tau)\big)y_i - \frac{e^2}{\pi\epsilon_0 m\Omega^2}\sum_j \frac{(y_j - y_i)}{r_{ij}^3} \quad (8)$$

and

$$\frac{d^2z_i}{d\tau^2} = 2\big(a - 2q\cos(2\tau)\big)z_i - \frac{e^2}{\pi\epsilon_0 m\Omega^2}\sum_j \frac{(z_j - z_i)}{r_{ij}^3} \quad (9)$$

Here, x_i, y_i, and z_i are the Cartesian coordinates of the ith ion, and r_{ij} signifies the distance between ions i and j.

III. Model for the Simulation of Trapped-Ion Dynamics

Equations (7), (8), and (9) completely describe the trapping and interparticle Coulomb effects on each ion in a cloud of arbitrary size. Because the interest here is the low-temperature behavior of collections of ions, a damping that is proportional to particle velocity is introduced in order to cool the ions. This adds a final term to the differential equations

$$\frac{d^2x_i}{d\tau^2} = -\big(a - 2q\cos(2\tau)\big)x_i - \frac{e^2}{\pi\epsilon_0 m\Omega^2}\sum_j \frac{(x_j - x_i)}{r_{ij}^3} - \frac{2\mathcal{D}}{\Omega}\frac{dx_i}{d\tau} \quad (10)$$

$$\frac{d^2y_i}{d\tau^2} = -\big(a - 2q\cos(2\tau)\big)y_i - \frac{e^2}{\pi\epsilon_0 m\Omega^2}\sum_j \frac{(y_j - y_i)}{r_{ij}^3} - \frac{2\mathcal{D}}{\Omega}\frac{dy_i}{d\tau} \quad (11)$$

and

$$\frac{d^2z_i}{d\tau^2} = 2\big(a - 2q\cos(2\tau)\big)z_i - \frac{e^2}{\pi\epsilon_0 m\Omega^2}\sum_j \frac{(z_j - z_i)}{r_{ij}^3} - \frac{2\mathcal{D}}{\Omega}\frac{dz_i}{d\tau} \quad (12)$$

where $\mathcal{D}$ is a coefficient of the damping. Once again, the factor of $2/\Omega$ in the third term of each of these equations appears because of the change of variable to dimensionless time τ. The inverse of the damping coefficient $1/\mathcal{D}$ is known as the damping time τ_d of a system with damping $\mathcal{D}$.

In a manner similar to the case of particles undergoing Brownian motion, a random walk in velocity is introduced, which simulates the process that sustains ion motion in the presence of damping, thus preventing the temperature from reaching zero. The growth in kinetic energy stemming from this random-walk step in velocity is balanced by the velocity damping introduced in the above equations of motion. This balance determines the size of the random-walk step that yields the desired final temperature.

The signature of a random-walk progression is that the mean square of the quantity in question increases linearly with the number of steps $\mathcal{N}$ in the walk [6]. Here, this quantity will be a velocity in the space of the dimensionless parameter τ, denoted as

$$v_\tau = \frac{dx}{d\tau}$$

Thus, the magnitude of the random-walk step in the dimensionless time space Δv_τ must obey

$$< v_\tau^2 > = \mathcal{N}(\Delta v_\tau)^2 \quad (13)$$

or in terms of the usual velocity v,

$$< \left(\frac{dx}{d\tau}\right)^2 > = \frac{4}{\Omega^2} < \left(\frac{dx}{dt}\right)^2 > \quad (14)$$

$$= \frac{4}{\Omega^2} < v^2 > = \mathcal{N}(\Delta v_\tau)^2 \quad (15)$$

Introducing a short dimensionless time interval h between random-walk steps so the $\mathcal{N}$ steps of length h represent a span of dimensionless time τ,

$$\frac{4}{\Omega^2} < v^2 > = \frac{\mathcal{N}h}{h}(\Delta v_\tau)^2 = \tau\frac{(\Delta v)^2}{h} \quad (16)$$

and, hence,

$$\left(\frac{d < v^2 >}{d\tau}\right)_{rw} = \frac{\Omega^2}{4}\frac{(\Delta v)^2}{h} \quad (17)$$

where rw suggests that this is due to the random walk. This is no more than a restatement of the fact that the mean square of the velocity grows linearly in time in the random walk. The growth of $< v^2 >$ due to the random walk is balanced by the damping of velocity per the damping terms in Eqs. (10), (11), and (12). The term due to damping becomes

$$\frac{d(v^2)}{d\tau} = -\frac{4}{\Omega}\mathcal{D}v^2 \tag{18}$$

For this damping term, it can be shown that when the interval over which v^2 is averaged is small in comparison to $\tau_d/2$, $< v^2 >= v^2$. Then

$$\left(\frac{d < v^2 >}{d\tau}\right)_{damp} = \left(\frac{d(v^2)}{d\tau}\right)_{damp}$$

$$= -\frac{4}{\Omega}\mathcal{D} < v^2 > \tag{19}$$

Setting the sum of the two terms to zero to balance the effects yields

$$\frac{d < v^2 >}{d\tau} = \left(\frac{d < v^2 >}{d\tau}\right)_{rw} + \left(\frac{d < v^2 >}{d\tau}\right)_{damp}$$

$$= \frac{\Omega^2}{4}\frac{(\Delta v_\tau)^2}{h} - \frac{4}{\Omega}\mathcal{D} < v^2 >= 0 \tag{20}$$

To get a random direction of the change in velocity, a separate random walk is taken in each of the Cartesian directions x, y, and z. Therefore, the Δv_τ in Eq. (20) is the size of the step in any one of these dimensions, and v^2 is the velocity squared in any one dimension. The temperature T of the system is introduced by use of the equipartition of energy

$$\frac{1}{2}k_B T = \frac{1}{2}m < v^2 >$$

Making this substitution for $< v^2 >$ and solving for Δv_τ in Eq. (20) yields the magnitude of the random-walk step in one dimension:

$$\Delta v_\tau = \sqrt{\frac{16\mathcal{D}hk_B T}{m\Omega^3}} \tag{21}$$

The sign of this velocity boost is determined by using a random-number generator that chooses each sign 50 percent of the time.

The approach to simulating a system described by these equations is obviously to determine the time evolution of the position–momentum states of the particles. The necessity of a constant small time step h in the random-walk formulation of temperature creates an ideal situation in which to use a fourth-order Runge-Kutta integration, with a constant time step, of the differential Eqs. (10), (11), and (12). The time between the random-walk steps h will also be the time step of the integration routine, so that the random walk can be executed at each integration step. The only requirement on the size of h is that it is small enough so that the errors (of the order h^5) are "small enough." In the case that the Runge-Kutta integration is calculating a specific numerical solution, one checks the solution by cutting h in half and checking that the two solutions agree [7]. In the case described here, where the integration is producing the motion of the ions in time, the appropriateness of the size of h can be checked by determining that halving h does not produce any noticeable increase in smoothness of the motion. In the cases examined, it was found that an integration step of 1/20 the period of the rf-driven motion, $h = 2\pi/20\Omega$, gives the desired precision.

The integration will give the three components of position and velocity for each particle at each step of the integration. This position–momentum state contains all the information about the system; other descriptions of the system are just obtained from the position–momentum state as appropriate. For instance, to obtain a kinetic energy for the entire cloud at any given time, the velocities of each particle are used to compute $mv^2/2$, and summing this quantity over each particle in the cloud gives an instantaneous total kinetic energy.

IV. Comparison of Results of the Model With Theory

Verification that the modeling of trapping voltages and Coulomb interactions is an accurate representation of a system of ions in a trap can be performed by checking the behavior of ions in situations readily calculable from the equations of motion. For instance, it was previously mentioned that an ion in the rf field oscillates with a slow secular motion in addition to the fast driven motion (the "micromotion"). The secular frequencies are given by [8] as

$$\omega_r^2 = \frac{e^2 V_{AC}^2}{2m^2\Omega^2 r_0^4} + \frac{eV_{DC}}{mr_0^2} \tag{22}$$

and

$$\omega_z^2 = \frac{2e^2V_{AC}^2}{m^2\Omega^2r_0^4} - \frac{2eV_{DC}}{mr_0^2} \tag{23}$$

These quantities are easily calculated for any combination of the trapping voltages. In particular, if either V_{AC} or V_{DC} is zero, the expressions for secular frequencies reduce to a single term. Another simple case for which this happens is the so-called "spherical" case often employed in trap operation, in which ω_r^2 and ω_z^2 are chosen to be equal by setting

$$V_{DC(sph)} = \frac{eV_{AC}^2}{2m\Omega^2r_o^2} \tag{24}$$

which gives

$$\omega_r^2 = \omega_z^2 = \frac{e^2V_{AC}^2}{m^2\Omega^2r_0^4} \tag{25}$$

To isolate the trapping and Coulomb forces, the parameters $\mathcal{D}$ and T in Eqs. (10), (11), (12), and (21) are simply set to zero. Then a simulation of a single ion in the trap clearly shows the micromotion (if $V_{AC} \neq 0$) and the slower secular oscillation, as in Fig. 2. The period of the oscillation can then be found by measuring the time between three successive zero-crossings of the position versus time graph. Since the position data exist only at each integration step h, the location in time of a zero-crossing is determined only to the accuracy of $\pm\frac{1}{2}h$.

The values obtained from the simulation of the periods T corresponding to these frequencies and the corresponding values from the above theory are summarized in Table 1. The agreement of the periods and the smooth sinusoidal motion seen in Fig. 2 indicate that the integration of the trapping and Coulomb terms is working properly.

If the temperature parameter accurately models ordinary temperature in kelvins, then, as previously suggested, the particles should have a thermal energy of $\frac{1}{2}k_BT$ per degree of freedom. This can be checked in the simulation by computing the mean-square velocity of the guiding center of motion, that is, a $< v^2 >$ that does not include the driven micromotion of the particles. This is done by computing the motion in time of the average position of each particle over a micromotion period, and then averaging the square of this quantity over all ions and over a satisfactory span of time.

For various degrees of damping and number of ions N_{ions}, the computational value of v^2 is in agreement with the theoretical value given by the equipartition of energy, as summarized in Table 2 for $T = 0.005$ K and $m = 137$ atomic mass unit (amu). The uncertainties reported are computed as the standard deviation in the N measurements.

The theoretical value is within the uncertainty range of each of the computational values. This indicates that a random walk in velocity space is a valid model of temperature.

V. Comparison of the Results of the Model With Experiments

Another way to examine the validity of using this simulation is to compare the ion dynamics with results observed by experimenters who have trapped charged micron-sized particles in an rf trap. Using a suitable magnification method, these particles can be observed visually or photographed. Thirty-two particles trapped with an rf field only ($V_{DC} = 0$) have been seen to have a "crystalline" state where the particles arrange themselves in three concentric circles containing 4, 14, and 14 particles [4]. This photograph is shown in Fig. 3(a); the appearance of each particle as a line is due to the fast micromotion. Simulating this situation gives a similar "photograph" when the x–y positions of all particles are plotted over one period of the micromotion, Fig. 3(b).

When $V_{DC} \neq 0$ and there are many ($\approx$100) charged particles in a dust trap, experimenters have seen a characteristic picture in which the large micromotion of the particles farthest away from the node maps out the electric field pattern of the trap, as shown in Fig. 4(a) [4]. In a simulation of 128 particles, the plot of their motions in three dimensions yields a similar picture, Fig. 4(b).

Experiments in which small numbers of ions in an rf trap are caused to visibly fluoresce have been carried out [9]. These experiments indicate that with $V_{DC} = 0$, a pair of ions has a stable configuration in which the pair is situated symmetrically about the node in the $z = 0$ plane, Fig. 5(a). With $V_{DC} > V_{DC(sph)}$, however, the z direction is preferred, and the most stable configuration is with the pair centered about the node in the $r = 0$ plane, Fig. 5(b). These results may be understood from the use of a harmonic pseudopotential that is derived through the force on a trapped particle averaged over one rf cycle [2]: in the first case, with $V_{DC} = 0$, the restoring force in the pseudopotential well is four times as strong in the r direction as in the z direction. However, in the case that $V_{DC} > V_{DC(sph)}$, the force is stronger in the axial (z) direction.

Duplicating these situations in the simulation produces the same most stable configuration in each case. Furthermore, the nature of the potential well is evident in noting the progress of the system toward this configuration when the initial conditions are far from it. For instance, the ions may be started on the $z = 0$ plane, with the voltages set in the $V_{DC} > V_{DC(sph)}$ case. Note that by Eq. (2), there is no trapping force in the z direction on a particle situated at $z = 0$. Hence, the trapping force alone would never bring the particles out of the $z = 0$ plane no matter how deep the well in the z direction! In the actual system, of course, collisions with the atoms of the buffer gas will knock the ions off the plane, allowing the force to have nonzero components in both directions. The ions can then drop into the well.

It is evident that in a computer model, some noise that can mix the r and z directions in this way must be included [10]; in the simulation described here, the random walk in velocity provides this noise. Starting the ions centered about the node on the $z = 0$ plane produces motion as shown in Fig. 6, which is obtained by plotting the positions of the two ions when they are near the maxima of their secular oscillation for several secular periods. Initially the ions oscillate only in the r direction; then the random-walk step moves the ions off the $z = 0$ plane. Note the symmetry of the system: the ions stay opposite one another as if connected by a spring, as suggested by the dashed lines between the pairs of ions. Now that the trapping force has both r and z components, the ions can move toward their most stable configuration along the z axis. They "overshoot" the z axis due to the angular momentum they have from being drawn toward the axis, and then return, precessing about the axis in this manner (suggested by the solid arrows) until the motion is damped out and the ions sit quite stably along the axis with only slight vibrations around their equilibrium positions (Fig. 7).

VI. Comparison to Other Simulations

Although there are no other large-scale simulations of rf traps, simulations [12] of large numbers of ions in a Penning trap have been conducted. These are based on the notion that, disregarding the motion due to the confining fields, confined ions are regarded as thermal particles with a mutual Coulomb repulsion in either type of trap. This repulsion keeps the ions quite far apart from one another, similar to states observed in a one-component plasma [11].

A useful way to describe the energy state of a plasma is by its coupling constant Γ, which is the ratio of Coulomb energy to thermal kinetic energy, or e^2/ak_BT. Here a is an average distance between the ions, k_B is the Boltzmann constant, and T is temperature.

If Γ is $<< 1$, the thermal energy is much greater than the Coulomb energy, and the ions may be expected to move quite freely as thermal particles without much regard to the comparatively weaker Coulomb force. However, if $\Gamma >> 1$, the Coulomb energy exceeds the kinetic energy, and less thermal motion would be expected in the ion system. The theory predicts a solid-like state with very little thermal motion for $\Gamma \geq 180$, and a liquid-like state with an intermediate level of thermal diffusion for $2 \leq \Gamma \leq 180$ [5].

The Penning trap simulations have shown that in the spherical case, when the coupling Γ between the ions is large, the ions form into concentric spherical shells centered on the trap node. Qualitative agreement, with the exception in some cases of the presence of cylindrical shells rather than spheroids, is seen in actual experiments on many Penning-trapped ions, which can be visually observed by causing the ions to fluoresce [13].

The simulation described here has also shown this behavior for ion clouds of up to 512 ions. This is shown in Figs. 8(a), (b), and (c) for several cloud sizes by plotting the positions of the ions in two dimensions as $|z|$ versus $\sqrt{x^2 + y^2}$. This picture has the effect of sweeping around all ϕ (the longitudinal angle in spherical coordinates) and folding into one quadrant. Using this representation, the adding of additional shells with increasing numbers of ions due to their Coulomb repulsion is clear: 128 ions arrange themselves in three shells, 256 ions in four shells, and for 512 ions a fifth shell is necessary. By taking the "photograph" during the crystallization process, information is gained on the process itself. It is seen in Fig. 9 that in this 512-ion case, the ion density begins to build up on what will be the fifth (outer) and the fourth shells in Fig. 8(b) while the ions are still mixing with respect to one another.

It has been reported that for very large Γ, the ions on the outer shell of a large ion cloud will have very little thermal motion, in accordance with the strongly coupled plasma theory. Furthermore, these ions arrange themselves into a two-dimensional hexagonal lattice on the surface of the shell [12]. The simulation described here also produces this result in both 128- and 256-ion clouds. The lattice itself can be examined in a polar plot (θ versus ϕ) as in Fig. 10(a), or in a "time-lapse" three-dimensional plot of ions on the hemisphere, Fig. 10(b).

The lattice can also be examined in a more quantitative fashion by considering the spatial correlation of the ions on the outer shell. The coordination number function $C(s)$

describes the average number of ions within a distance s of one ion, and the correlation function $c(s)$ is given in terms of $C(s)$ as [12]

$$\int_0^s 2\pi s c(s) ds = C(s) \tag{26}$$

A regular two-dimensional hexagonal lattice has six nearest neighbors to any one point, and eighteen next-nearest neighbors, so the function $C(s)$ when plotted against s should show horizontal shoulders at $C(s) = 6$ and $C(s) = 18$. The correlation function can be obtained from $C(s)$ by Eq. (26).

For the 128-ion cloud in Figs. 10(a)–10(d), which is at $\Gamma = 556$, the highly regular hexagonal lattice is evident in the polar plot and the three-dimensional plot, and supported by the shape of $C(s)$, Fig. 10(c). The correlation function itself, $c(s)$, has three smooth, well-defined peaks, Fig. 10(d), which also indicates a large degree of order.

At $\Gamma = 139$, some changes in the lattice are evident in the three-dimensional plot (Fig. 11). This time-lapse plot shows that over a length of time, the ions wander quite a bit more from their positions in the hexagonal lattice, but there is still a fair degree of order and there is not much exchanging of positions between ions.

When Γ is lowered to 65, the time-lapse plot shows that the ions are wandering quite randomly over the surface of the sphere, Fig. 12(a). Indeed, the second shoulder of $C(s)$ has been virtually wiped out, Fig. 12(b), indicating that order exists only on the scale of the first unit cell. The plot of $c(s)$ has similarly degraded, Fig. 12(c). The simulations that have been done on Penning trap systems also show this effect, in which the ions are crystallized into shells but diffuse freely over the surface of the shell, for low (but > 1) values of Γ [12].

VII. Conclusions

It has been shown that this model of the Paul trap system gives results that agree with trapping theory, visual observations of trapped particles, and other computer simulations of trapped charged particles. Armed with this model, questions that are important to the trapped-ion frequency standard can now be examined, such as the effect of "rf heating," in which a large ion cloud may gain extra energy from the effects of the trapping rf field [14]. Clearly, the normal modes of oscillation of a system of N ions in this rf quadrupole field have not been solved analytically; the simulation may be an excellent way to understand the oscillations of such a large system. Also, by simply revising the differential equations in the computer program, rf simulations of other trap geometries (such as the linear ion trap described in [8], which is now in use) can be done.

To the authors' knowledge, there have been no simulations of ions in such a linear trap, and although experiments have been done at JPL on the confinement of micron-sized particles in a linear trap, they are not nearly as detailed as the studies in [4], and little is known about the crystalline structures that may form in a linear trap. Therefore, it is indeed important to have confidence in the integrity of the simulation by examining a system that has been widely studied (the hyperbolic trap) before progressing to less understood systems.

Acknowledgments

The authors wish to acknowledge the use of the JPL and NASA Ames Numerical Aerodynamic Simulation supercomputers to perform these simulations.

References

[1] A. Williams, R. Melbourne, L. Maleki, G. Janik, and J. Prestage, "An Apparatus for the Electrodynamic Containment of Charged Macroparticles," *TDA Progress Report 42-98*, vol. April–June 1989, Jet Propulsion Laboratory, Pasadena, California, pp. 57–62, August 15, 1989.

[2] H. G. Dehmelt, *Advanced Atomic Molecular Physics*, Vol. III: New York: Academic Press, 1967.

[3] D. J. Wineland, "Spectroscopy of Stored Ions," *Precision Measurement and Fundamental Constants II*, U. S. National Bureau of Standards, Special Publication 617, pp. 83–92, Boulder, Colorado, 1984.

[4] R. F. Wuerker, H. Shelton, and R. V. Langmuir, "Electrodynamic Containment of Charged Particles," *J. Appl. Phys.*, vol. 30, no. 3, pp. 342–349, March 1959.

[5] J. J. Bollinger and D. J. Wineland, "Microplasmas," *Scientific American*, vol. 262, no. 1, pp. 124–130, January 1990.

[6] P. M. Morse, *Thermal Physics*, New York: W. A. Benjamin, Inc., 1969.

[7] G. Arfken, *Mathematical Methods for Physicists*, Orlando, Florida: Academic Press, Inc., 1985.

[8] J. D. Prestage, G. J. Dick, and L. Maleki, "New Ion Trap for Frequency Standard Applications," *J. Appl. Phys*, vol. 66, no. 3, pp. 1013–1017, August 1, 1989.

[9] D. J. Wineland, J. C. Bergquist, Wayne M. Itano, J. J. Bollinger, and C. H. Manney, "Atomic-Ion Coulomb Clusters in an Ion Trap," *Phys. Rev. Lett.*, vol. 59, no. 26, pp. 2935–2938, December 28, 1987.

[10] J. Hoffnagle, R. G. DeVoe, L. Reyna, and R. G. Brewer, "Order-Chaos Transition of Two Trapped Ions," *Phys. Rev. Lett.*, vol. 61, no. 3, pp. 255–258, July 18, 1988.

[11] J. H. Malmberg and T. M. O'Neil, "Pure Electron Plasma, Liquid, and Crystal," *Phys. Rev. Lett.*, vol. 39, no. 21, pp. 1333–1336, November 21, 1977.

[12] D. H. E. Dubin and T. M. O'Neil, "Computer Simulation of Ion Clouds in a Penning Trap," *Phys. Rev. Lett.*, vol. 60, no. 6, pp. 511–514, February 8, 1988.

[13] S. L. Gilbert, J. J. Bollinger, and D. J. Wineland, "Shell-Structure Phase of Magnetically Confined Strongly Coupled Plasmas," *Phys. Rev. Lett.*, vol. 60, no. 20, pp. 2022–2025, May 16, 1988.

[14] H. Dehmelt, in *Advances in Laser Spectroscopy*, F. T. Arecchi, F. Strumia, and H. Walther, editors, New York: Plenum, pp. 153–188, 1983.

Table 1. Comparison of secular oscillation periods

V_{AC}	V_{DC}	Computational T_r	Theoretical T_r	Computational T_z	Theoretical T_z
120	0	1048 ± 1	1048.0	523 ± 1	524.0
0	40	211 ± 1	210.9	149 ± 1	149.1
120	$V_{DC(sph)}$	740 ± 1	741.0	740 ± 1	741.0

Note: Voltages are reported in volts, and periods in integration steps, h.

Table 2. Comparison of thermal energies

N_{ions}	τ_d/τ_s	Computational v^2	Theoretical v^2	N
128	9.77	0.30079 ± 0.01475	0.301231	24
128	26.6	0.27942 ± 0.02556	0.301231	26
256	4.9	0.29976 ± 0.00576	0.301231	19

Note: The value τ_d/τ_s is a measure of the relative amount of damping: the ratio of the damping time to the single-particle secular period.

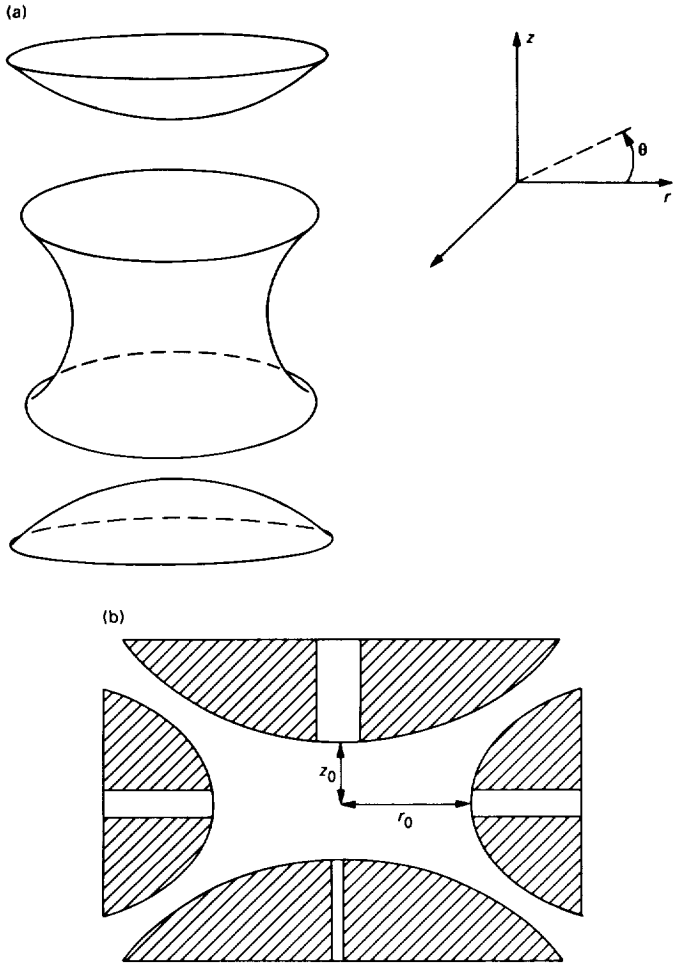

Fig. 1. A hyperbolic trap: (a) the three electrodes, consisting of one ring electrode and two endcaps, and (b) the assembled hyperbolic trap in cross section.

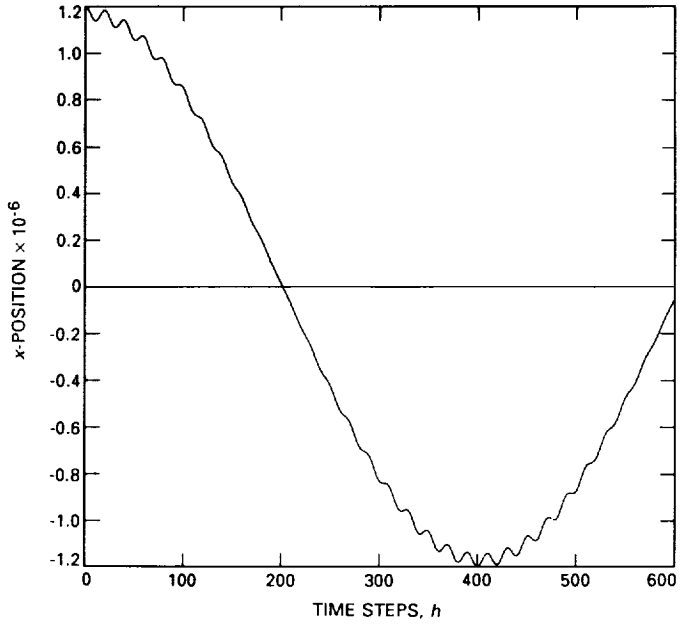

Fig. 2. One-dimensional single-particle trajectory in a Paul trap, showing the fast driven micromotion superimposed on the slower secular motion.

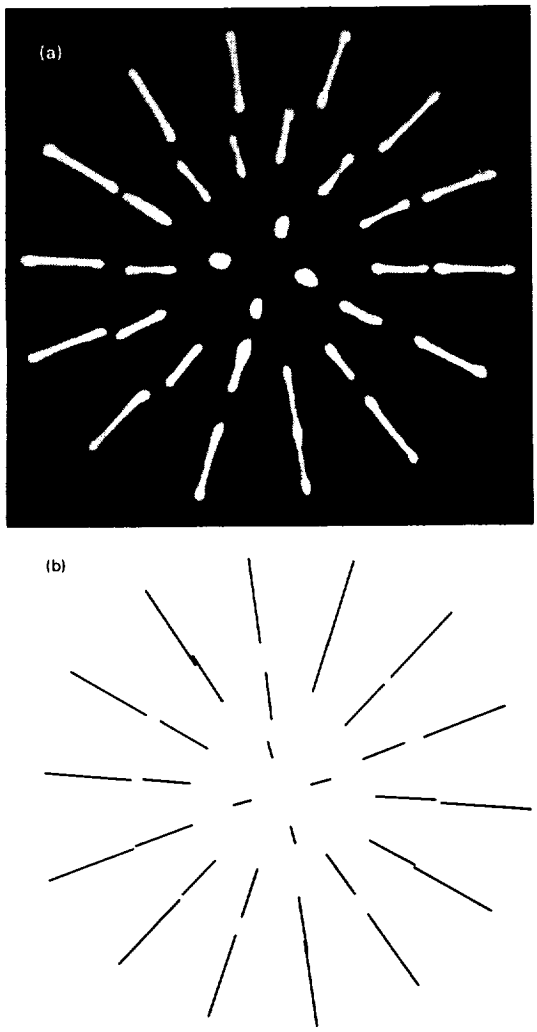

Fig. 3. Comparison of rf-trapped macroparticles with simulation: (a) photograph from [4] showing the "crystalline" state of 32 particles, and (b) results from the simulation of 32 trapped particles.

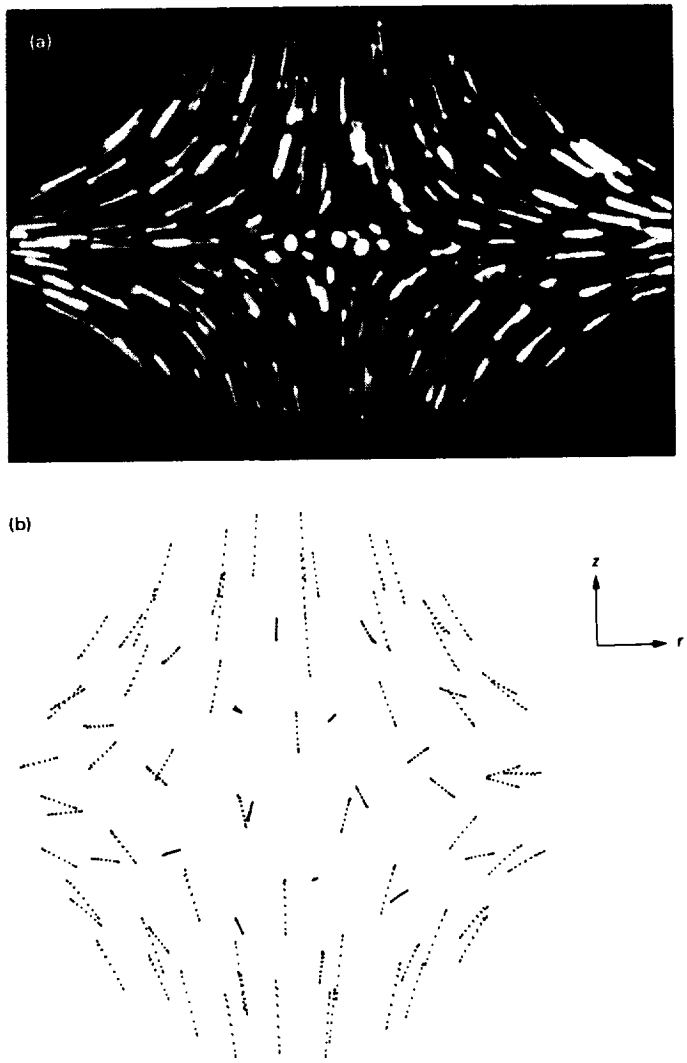

Fig. 4. Comparison of ≈100 rf-trapped particles with simulation: (a) photograph from [4] showing ≈100 particles outlining the fields in the trap, and (b) results from the simulation of 128 rf-trapped particles.

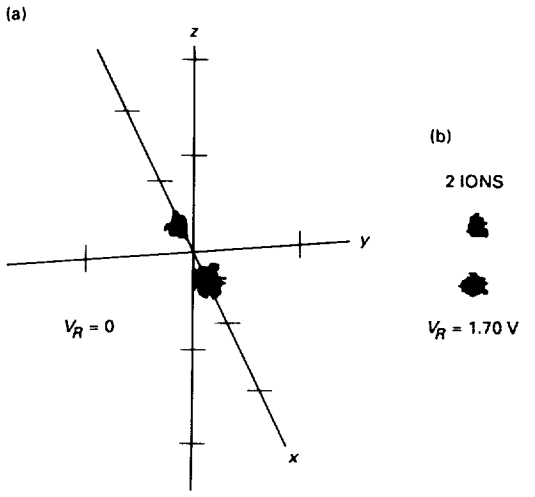

Fig. 5. Photograph from [9] showing two trapped ions whose preferred configuration is to be situated (a) symmetrically about the node in the radial direction, and (b) symmetrically about the node in the axial direction.

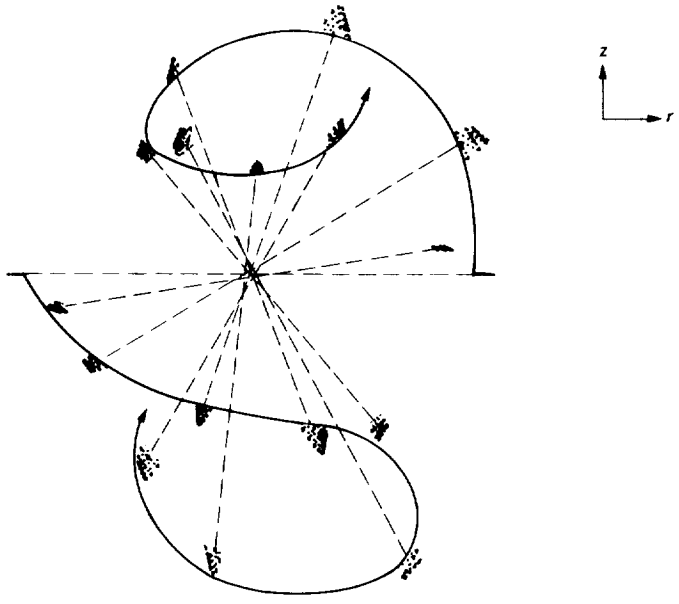

Fig. 6. Simulation of a pair of ions whose preferred configuration is to lie on the *z*-axis; when placed on a radial axis, they are drawn toward the vertical and precess about the *z*-axis.

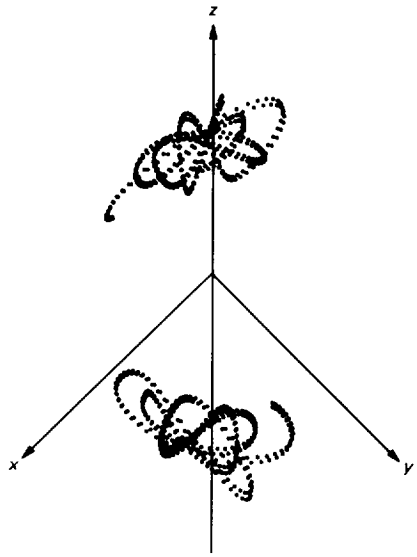

Fig. 7. The system of Fig. 6, after much of the precessional motion has damped out, sits stably along the *z*-axis.

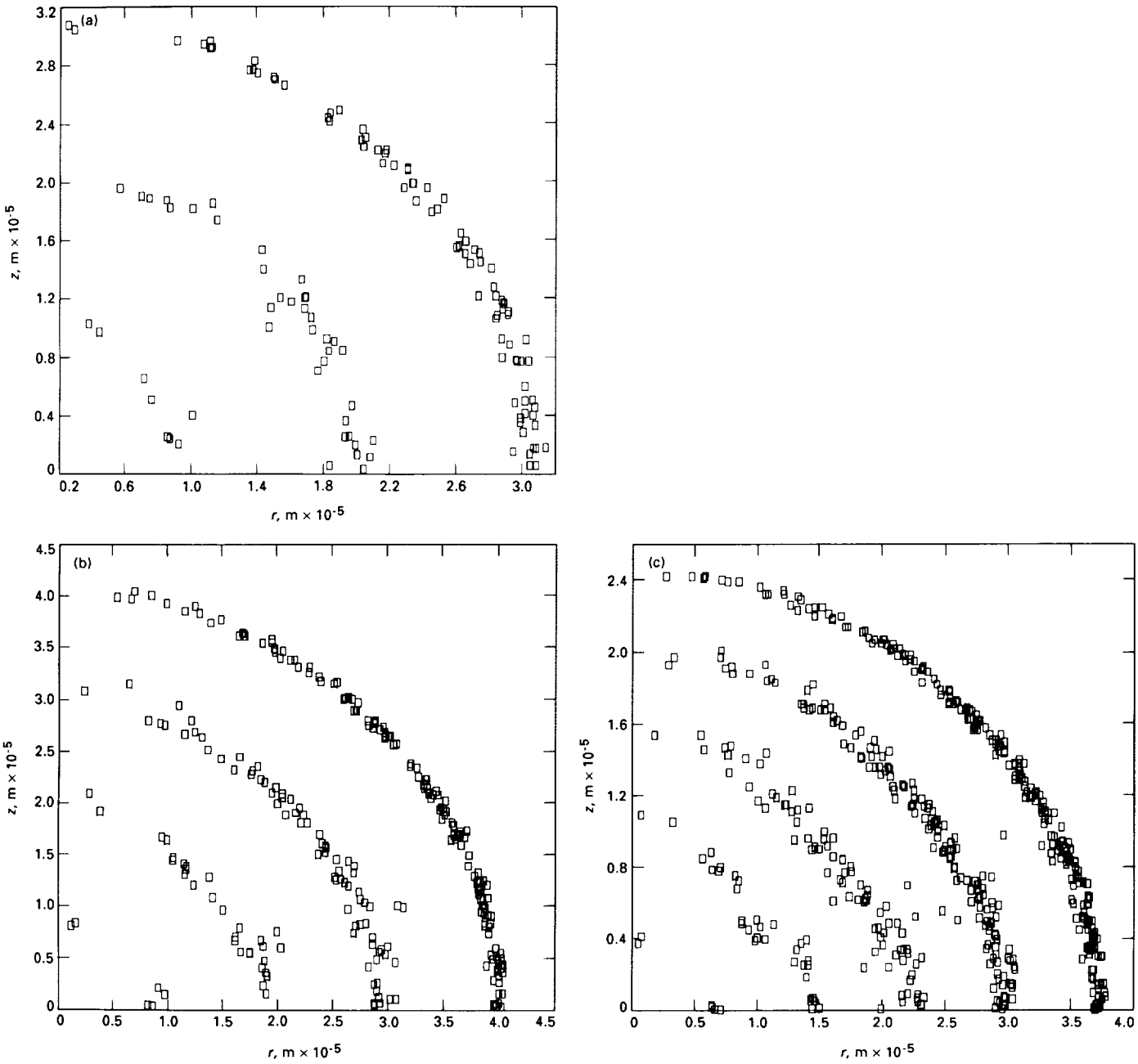

Fig. 8. An *r* versus *z* plot of the positions of ions in a simulation: (a) 128 ions form three concentric spherical shells; (b) 256 ions form four spherical shells; and (c) 512 ions form five spherical shells.

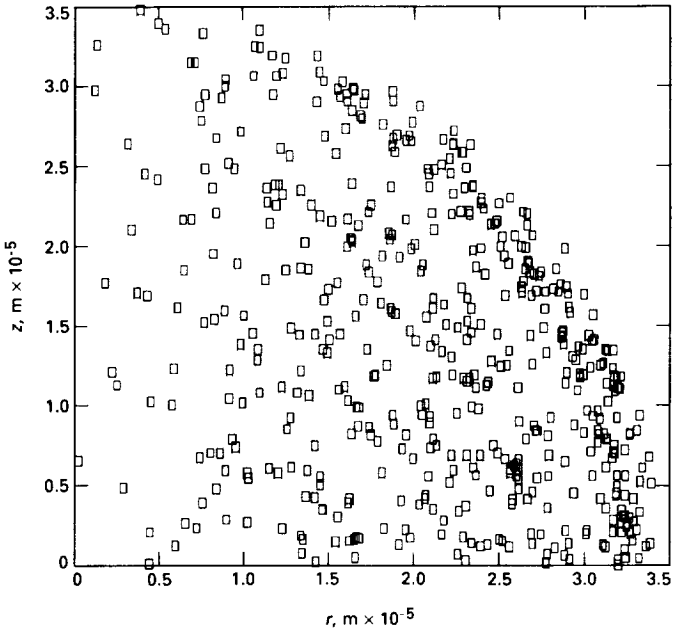

Fig. 9. An *r* versus *z* plot of a simulation of 512 ions during their crystallization, showing the buildup of density where the fourth and fifth shells are forming.

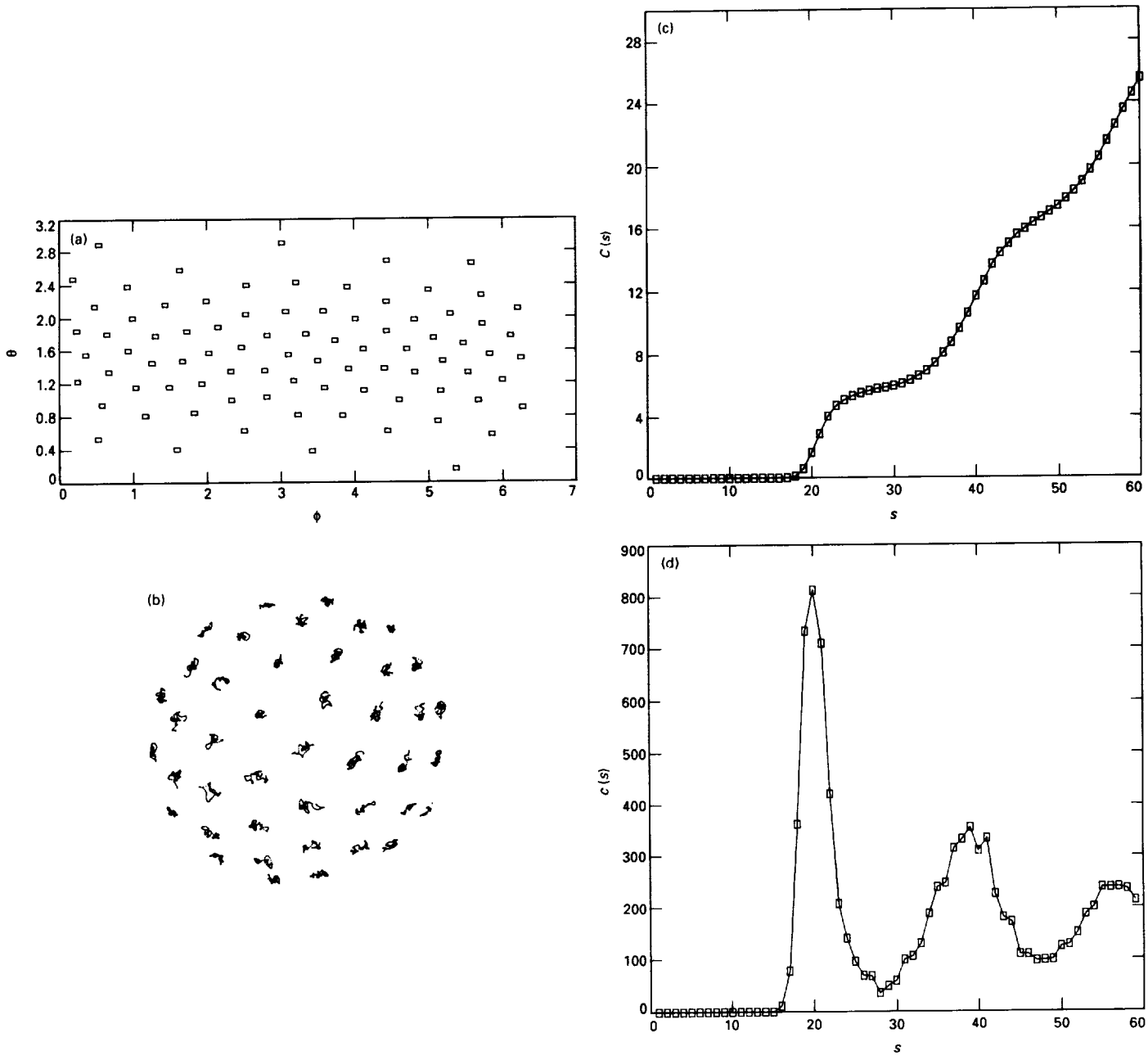

Fig. 10. A 128-ion cloud: (a) polar (θ versus ϕ) plot of ions on the outer shell at $\Gamma = 556$, showing the two-dimensional hexagonal lattice that forms on the surface of the shell; (b) three-dimensional view of ions on the near hemisphere of the outer shell (the positions on this "time-lapse" plot are sampled once per micromotion cycle); (c) the coordination number function $C(s)$ of the ions in the system of (a), showing shoulders at $C(s) = 6$ and $C(s) = 18$, indicating a hexagonal lattice; and (d) the correlation function $c(s)$ of this system. The three smooth, well-defined oscillations of this function indicate a high degree of order.

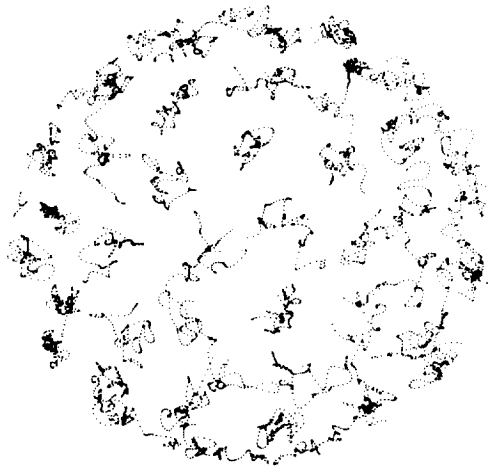

Fig. 11. Time-lapse plot similar to Fig. 10(b), showing the outer hemisphere of a 128-ion cloud at $\Gamma = 139$. More thermal motion is seen here than in Fig. 10(b).

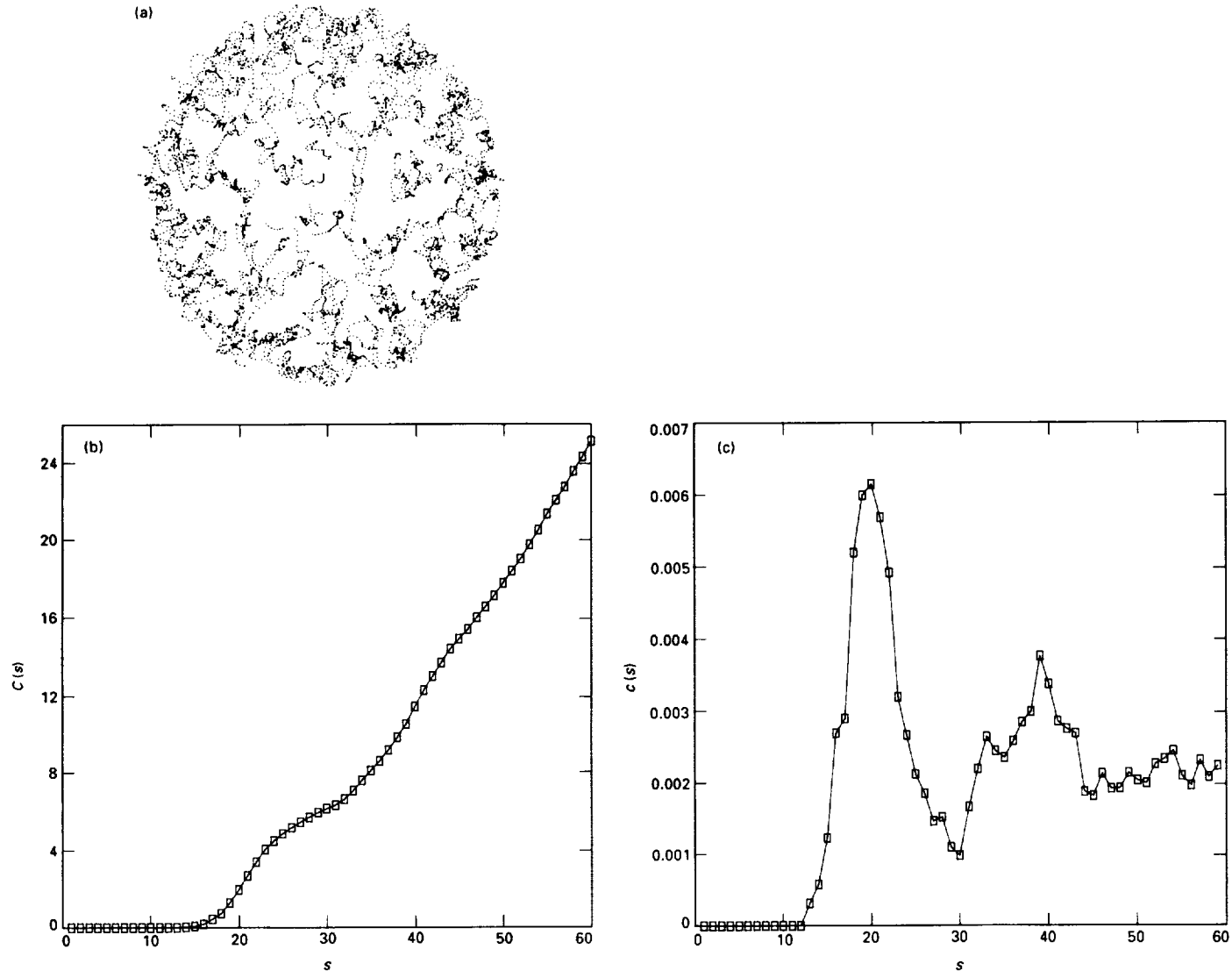

Fig. 12. A 128-ion cloud at $\Gamma = 65$: (a) time-lapse plot showing that the ions diffuse about the spherical shell much more in this case than at the higher values of Γ; (b) coordination number function $C(s)$ of the system of (a), showing that in comparison to Fig. 10(c) the shoulder at $C(s) \approx 18$ has disappeared, indicating that at this lower Γ order exists over length scales of a one-unit hexagonal cell only; and (c) correlation function $c(s)$ of this system. In comparison to the $c(s)$ in Fig. 10(d), this one is far noisier and lacks the third oscillation, indicating less order in this low-Γ system.